Journal of Superconductivity and Novel Magnetism (2025) 38:142
https://doi.org/10.1007/s10948-025-06981-0

RESEARCH

Rhombohedral Ba_2NbBO_6 (B = As, Sb, and Bi) Double Perovskites' Elastic, Thermodynamic, and Directional Thermoelectric Properties

Saber Saad Essaoud[1] · Missoum Radjai[2] · Abdelmadjid Bouhemadou[3] · Mohammed Elamin Ketfi[4] · Djamel Allali[5] · Rabah Khenata[6] · Yarub Al-Douri[7,8,9]

Received: 23 January 2025 / Accepted: 28 April 2025

Abstract
We systematically analyzed the elastic, thermodynamic, and directional thermoelectric properties of a set of double perovskites, specifically Ba_2NbAsO_6, Ba_2NbSbO_6, and Ba_2NbBiO_6. We investigated the dependence of volume, bulk modulus, thermal expansion coefficient, Debye temperature, entropy, isobaric and isochoric heat capacities, and lattice thermal conductivity on temperature and pressure using the quasi-harmonic Debye model. We analyzed the thermoelectric parameters, including the Seebeck coefficient, thermal and electrical conductivity of holes and electrons, figure of merit, and power factor, in the *xx*, *yy*, and *zz* directions, through the quasi-classical Boltzmann model. The findings demonstrate a figure of merit exceeding 0.8 across a wide range of charge carrier concentrations and a Seebeck coefficient greater than 0.9 mV/K, making Ba_2NbAsO_6, Ba_2NbBiO_6, and Ba_2NbSbO_6 compounds promising candidates for heat-to-electricity conversion applications. We assessed the mechanical stability and characteristics, including bulk modulus, shear modulus, Young's modulus, Poisson's ratio, Debye temperature, and the velocities of longitudinal, transverse, and average sound propagation, derived from the single-crystal elastic constants C_{ij}, which were evaluated numerically using the strain-stress technique.

Keywords Double perovskites · Ab initio calculations · Thermodynamic characteristics · Directional thermoelectric features

1 Introduction

The pivotal role of energy resources in vital economic and environmental areas has elevated the importance of investing in the quest for alternative energy sources. To accomplish this objective, theoretical and experimental research provided all of the data, experimental results, and theoretical coefficients necessary to improve and increase the quality of the most energy-oriented applications. This is particularly evident when manufacturing semiconductors with different

✉ Saber Saad Essaoud
saber.saadessaoud@univ-msila.dz

✉ Abdelmadjid Bouhemadou
abdelmadjid_bouhemadou@univ-setif.dz;
a_bouhemadou@yahoo.fr

[1] Laboratory of Materials and Renewable Energy, Department of Physics, Faculty of science, University of M'sila, University Pole, Road Bordj Bou-Arreridj, 28000 M'sila, Algeria

[2] Laboratory of Physics of Experimental Techniques and Their Applications (LPTEAM), University of Medea, Medea, Algeria

[3] Laboratory for Developing New Materials and their Characterizations, Department of Physics, Faculty of Science, Ferhat Abbas University - Setif 1, 19000 Setif, Algeria

[4] Department of Electronics, Faculty of Technology, University of M'sila, University Pole, Road Bordj Bou-Arreridj, 28000 M'sila, Algeria

[5] Faculty of Technology, University of M'sila, University Pole, Road Bordj Bou-Arreridj, 28000 M'sila, Algeria

[6] Laboratoire de Physique Quantique de la Matière et de Modélisation Mathématique (LPQ3M), Université de Mascara 29000, Mascara, Algeria

[7] College of Health and Medical Techniques, Al-Bayan University, Baghdad, Iraq

[8] Nanotechnology and Catalysis Research Center (NANOCAT), University of Malaya, 50603 Kuala Lumpur, Malaysia

[9] Department of Mechanical Engineering, Faculty of Engineering, Piri Reis University, Eflatun Sk. No: 8, 34940 Tuzla, Istanbul, Turkey

Published online: 07 May 2025

specifications and characteristics for photovoltaics, solar panels, thermoelectric generators, control devices, electrical transformers, optical and thermal sensors, etc. The experiments carried out to improve the performance of photovoltaic and thermoelectric devices have, in fact, given us important indications on how to choose the semiconductors used in these devices [1–6]. Double perovskite materials are among the materials that have shown semiconducting behavior with energy bandgaps and features that make them suitable for use as thermoelectric converters or in photovoltaic applications. X-ray diffraction (XRD), Fourier transform infrared (FTIR), and energy-dispersive spectroscopy (EDS) tests on $Pb_{0.5}Ba_{1.5}BiNbO_6$ show that this material has an orthorhombic structure and is a pure compound without any other particles. It exhibits a high dielectric constant and semiconducting behavior, with an optical band gap of 2.08 eV, making it suitable for blue LED applications [7]. Kai-qi et al. [8] reported that the maximum limited spectroscopic efficiency is approximately 31.9% for the lead-free $Cs_2AgInBr_6$ and about 32.45% for the lead-free $Cs_2AgGaBr_6$. This efficiency was achieved at a thickness of 1.5 µm and an electron mobility up to 160.8 $cm^2V^{-1}s^{-1}$, which is comparable to that of $MAPbI_3$ (165 $cm^2V^{-1}s^{-1}$). Additionally, some research showed that certain perovskite compounds exhibit enhanced performance in photo-thermal catalysis[9]. An experimental study conducted by Matli et al. [10] enabled the synthesis of La_2MMnO_6 ceramics (M = Ni or Co) using microwave fast sintering, which improved the magnetic and dielectric properties of the prepared compounds. Moreover, Lu et al. [11] synthesized the double perovskite compound $Sm_{0.7}Sr_{0.3}BaCo_2O_{5+\delta}$ at low cost by using the sol-gel method and high-temperature annealing. This makes this material affordable and possible to make on a large scale. The results of this work demonstrated that the double perovskite compound $Sm_{0.7}Sr_{0.3}BaCo_2O_{5+\delta}$ exhibits a broad absorption of the solar spectrum, reaching up to 93%with low thermal radiation loss compared to conventional carbon absorbers [11]. Furthermore, the use of this compound in an evaporator recorded an evaporation efficiency of 86% at a light density of 2 W/cm^2, which highlights its capacity to efficiently convert solar energy into thermal energy and enhances its suitability as a potential alternative to conventional materials in solar evaporation systems [11]. Ishfaq et al. demonstrated the efficacy of various double perovskite materials in thermoelectric conversions [12]. The results indicated that Sr_2LaTaO_6 and Sr_2LuTaO_6 had a figure of merit (ZT) value of 0.8 at or above ambient temperature [12], and other compounds, such as Ba_2CeSnO_6 and Ba_2CePtO_6, showed elevated Seebeck coefficients (S) of 170 and 221 µV/K at room temperature, respectively [13].

In addition to experimental investigations, many theoretical studies [14–24] have also focused on the study of double perovskite compounds, highlighting a wide range of materials in this family with a variety of crystal structures and intriguing properties such as optical, thermal, thermoelectric, mechanical, dynamic, and magnetic characteristics.

By applying the sate-of-the-art pseudopotential plane wave (PP-PW) and full-potential linearized augmented plane wave (FP-LAPW) methods, we performed an extensive predictive analysis of the elastic, thermodynamic, and directional thermoelectric characteristics of three double perovskites, Ba_2NbBO_6 (B = As, Sb, and Bi). We structure the paper as follows: in addition to this introduction, we briefly describe and explain the subtleties of the calculations before presenting and analyzing all the properties sought and concluding with a general summary.

2 Computational Approaches and Settings

First-principles calculations were performed using two complementary methods: the pseudopotential plane wave (PP-PW) method included in the quantum espresso package [25] and the full-potential linearized augmented plane wave (FP-LAPW) implemented in the WIEN2k code [26].

The explored compounds Ba_2NbAsO_6, Ba_2NbSbO_6, and Ba_2NbBiO_6 exhibit a rhombohedral crystallographic structure (Fig. 1) characterized by the symmetry group $R\bar{3}$ (No.

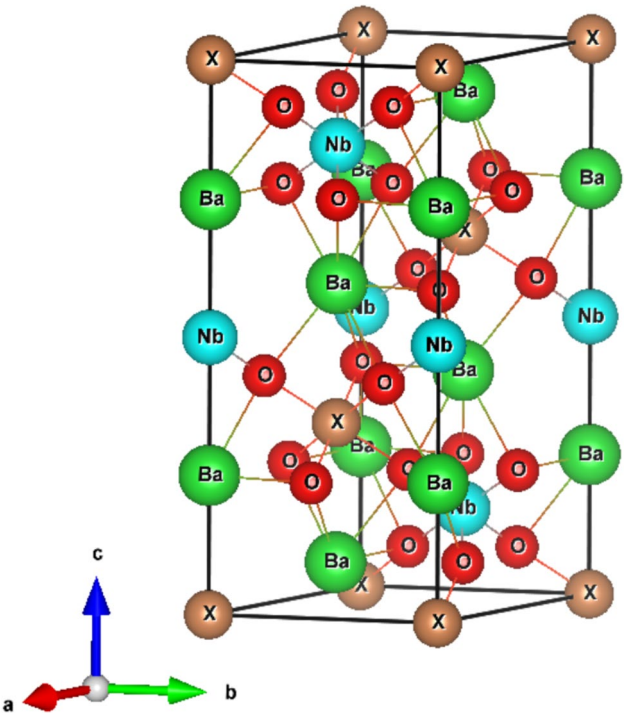

Fig. 1 A visual depiction of the rhombohedral configuration of the unit cell for the Ba_2NbXO_6 (X = As, Sb, and Bi) double perovskite materials using the VESTA software [39]

148).The equilibrium lattice parameters (a, c) determined using the PP-PW method with the GGA-PBEsol functional [27] are as follows: (5.844 Å, 14.293 Å) for Ba_2NbAsO_6, (6.004 Å, 14.544 Å) for Ba_2NbSbO_6, and (6.076 Å, 14.626 Å) for Ba_2NbBiO_6 [28]. Additionally, the thermodynamic stability of the three compounds was verified within a pressure range of -20 to 30 GPa, and their semiconductor properties were established with energy band gap values of 2.101 eV, 1.71 eV, and 2.813 eV for Ba_2NbAsO_6, Ba_2NbSbO_6, and Ba_2NbBiO_6, respectively [28]. The PP-PW calculations were performed using the following computational parameters: (i) a plane wave basis set with a cut-off energy of 480 eV, and (ii) a Brillouin zone sampling of $10 \times 10 \times 10$ k-points. The numerical evaluations of the elastic constants were accomplished using the energy-strain technique in combination with the FP-LAPW as implemented in the WIEN2k code. The FP-LAPW calculations were executed utilizing specific computational parameters: (i) the GGA-PBEsol functional when calculating the elastic constants, (ii) the Tran-Blaha modified-Becke-Johnson (TB-mBJ) potential [29] when calculating the thermoelectric properties, (iii) a plane wave basis set cut-off parameter $R_{MT}^{\min}K_{max} = 8$, and (iv) a Brillouin zone sampling with a $10 \times 10 \times 10$ k-point configuration.

The temperature dependence of the crystal thermal conductivity along the [100], [010], and [001] crystal directions was calculated using the phono3py program [30].

The Boltzmann transport model implemented in the BoltzTraP2 program [31] was combined with the FP-LAPW method to study the thermoelectric properties of the materials under consideration. The calculations employed a relaxation time of 10^{-14} s, the standard value used by the BoltzTraP2 program and widely accepted in numerous studies that utilize this software [31–36].

The quasi-harmonic Debye approximation incorporated in the GIBBS2 program [37, 38] was combined with the PP-PW method for the purpose of computing the thermodynamic characterizations.

3 Results and Discussion

3.1 Thermodynamic Characteristics

Based on quasi-harmonic Debye model, temperature and pressure dependencies of some macroscopic physical properties, namely the unit cell volume (V), bulk modulus (B), isochoric and isobaric heat capacities (C_V and C_P), entropy (S), volumetric thermal expansion coefficient (α), Debye temperature (T_D), and lattice thermal conduction (k_l) of the three examined compounds Ba_2NbBO_6 (B = As, Sb, and Bi) were predicted.

The temperature dependence of the unit cell volume (V) and bulk modulus (B) for Ba_2NbAsO_6, Ba_2NbSbO_6, and Ba_2NbBiO_6 over a temperatures range of 0–1000 K at constant pressures of 0, 20, and 40 GPa are illustrated in Fig. 2. Firstly, we notice a minor effect of temperature on these two quantities. Secondly, B rises gradually and in a linear manner as pressure increases, while V decreases slightly and in a linear manner increasing pressure. Pressure seems to exert a more substantial influence on both quantities examined than the impact of temperature. When the materials considered are subjected to a pressure of 20 GPa, the bulk moduli of Ba_2NbAsO_6, Ba_2NbSbO_6, and Ba_2NbBiO_6 increase by about 50 GPa, and their unit cell volumes decrease by about 80 $a.u^3$ ($a.u$: atomic unit).

Figure 2 illustrates the temperature dependence of the coefficient of volumetric thermal expansion (α) for the materials Ba_2NbAsO_6, Ba_2NbSbO_6, and Ba_2NbBiO_6 over the range of 0–1000 K at constant pressures of 0, 20, and 40 GPa. The temperature dependence of the thermal expansion coefficient (α) for the studied compounds mirrors the behavior of the isochoric heat capacity (C_V). Both quantities are directly proportional to the number of thermally activated vibrational modes, which increase with temperature. At low temperatures (below the Debye temperature, T_D), α and C_V scale proportionally to T^3, as dictated by the Debye T_D law. Beyond T_D, the thermal expansion coefficient continues to rise gradually, while the heat capacity asymptotically approaches a constant value, the so-called Dulong-Petit limit. This divergence reflects the distinct temperature-dependent contributions of vibrational modes to each property above the Debye regime. The volumetric thermal expansion coefficient values for the materials under investigation at 600 and 900 K surpass those of the double perovskites Ba_2MgWO_6 (3.56×10^{-5} K^{-1}) and Sr_2MgWO_6 (3.96×10^{-5} K^{1}), which were calculated within the temperature range of 298 to 1473 K [40].

The Slack model [41] was used to numerically evaluate the lattice thermal conductivity (k_l) for the materials under consideration. In the Slack model, the lattice thermal conductivity (k_l) is given as follows:$k_l = \frac{A\overline{m}V^{1/3}T_D{}^3}{\gamma^2 n_a{}^{2/3}T}$. In this context, $A = 2.43 \times 10^{-8}/(1 - 0.514/\gamma + 0.228/\gamma^2)$, $\overline{m}$ is the average atomic mass, n_a is the number of atoms in the primitive unit cell, V is the volume per atom, γ is the Grüneisen parameter, and T_D is the Debye temperature. When subjected to identical temperature and pressure, the lattice thermal conductivity values of Ba_2NbAsO_6, Ba_2NbSbO_6, and Ba_2NbBiO_6 are nearly equivalent. The lattice thermal conductivities of these compounds decrease considerably with increasing temperature, reaching values that do not exceed 0.2 $W.m^{-1}.K^{-1}$ for temperatures above 300 K at zero pressure. Unlike its temperature-dependent behavior, the lattice thermal conductivity increases with pressure. The lattice thermal conductivity of the three compounds considered increases

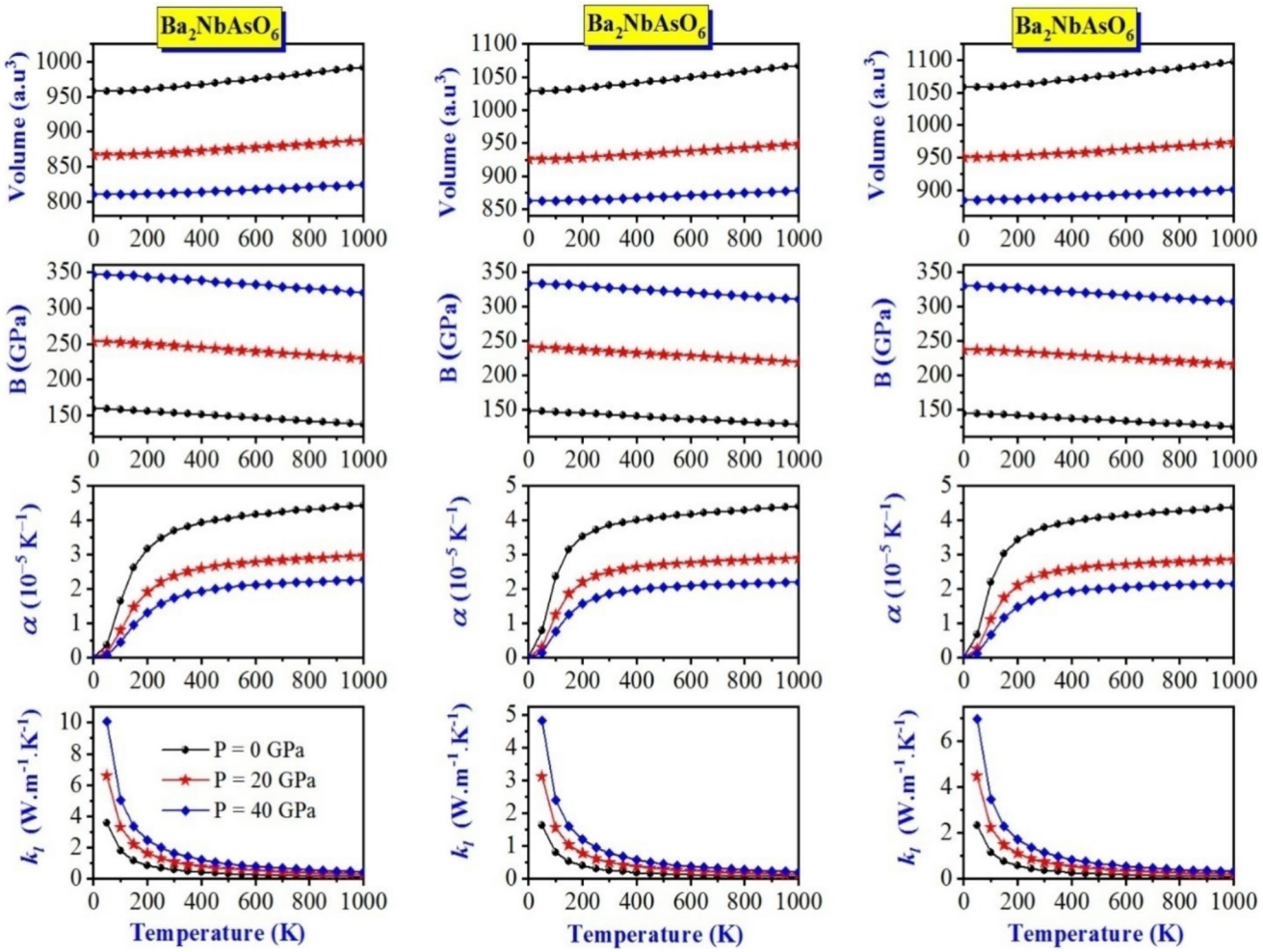

Fig. 2 Temperature dependency of the bulk modulus (B), unit cell volume (V), thermal expansion coefficient (α), and lattice thermal conductivity (k_l) of Ba_2NbAsO_6, Ba_2NbSbO_6, and Ba_2NbBiO_6 compounds at constant pressures of 0, 20, and 40 GPa

to about 3.0 $W.m^{-1}.K^{-1}$ at a temperature of 300 K and a pressure of 40 GPa.

Figure 3 illustrates the temperature dependence of the isochoric (C_V) and isobaric (C_P) heat capacities, entropy (S), and Debye temperature (T_D) for Ba_2NbAsO_6, Ba_2NbSbO_6, and Ba_2NbBiO_6 over a temperature range of 0–1000 K at constant pressures of 0, 20, and 40 GPa. Figure 3 illustrates a prompt rise in the C_V and C_P values as the temperature increases within the 0–300 K range. The C_V increase rate begins to slow down for temperatures above 300 K, tending towards the Dulong-Petit limit [42], which is equal to 250 $J.mol^{-1}.K^{-1}$. C_V nearly reaches this limit when the temperature exceeds 600 K. It is important to note that C_P does not converge to the Delong-Petit limit; it continues to increase even at temperatures exceeding 600 K. The effect of pressure on C_V and C_P is the opposite of the effect of temperature; C_V and C_P decrease with increasing pressure. This phenomenon is explained by the fact that pressure limits the movement and vibration of atoms, thus reducing their capacity to absorb energy. Among the three compounds under study, Ba_2NbSbO_6 exhibits a greater capacity for absorbing thermal energy due to its larger heat capacity than Ba_2NbAsO_6 and Ba_2NbBi_6.

The Debye temperature of a material is a key thermal parameter related to various critical material characteristics, such as hardness, thermal insulation, electrical insulation, thermal conductivity, thermal stability, thermal expansion, and flexibility [43, 44]. The obtained Debye temperature value at 300 K for Ba_2NbAsO_6 was greater than those of the $Sr_{2-x}La_xCoNbO_6$ compounds ($x = 0.4$ and 0.6), which were experimentally determined to be 353 K [45].

Figure 3 illustrates that the Debye temperatures (T_D) of Ba_2NbAsO_6, Ba_2NbSbO_6, and Ba_2NbBiO_6 decrease slightly with rising temperature but increase significantly with increasing pressure. For instance, when the pressure is raised to 20 GPa, the Debye temperatures of the mentioned compounds increase by approximately 90 K. Based on the T_D values, Ba_2NbAsO_6 demonstrates greater stiffness,

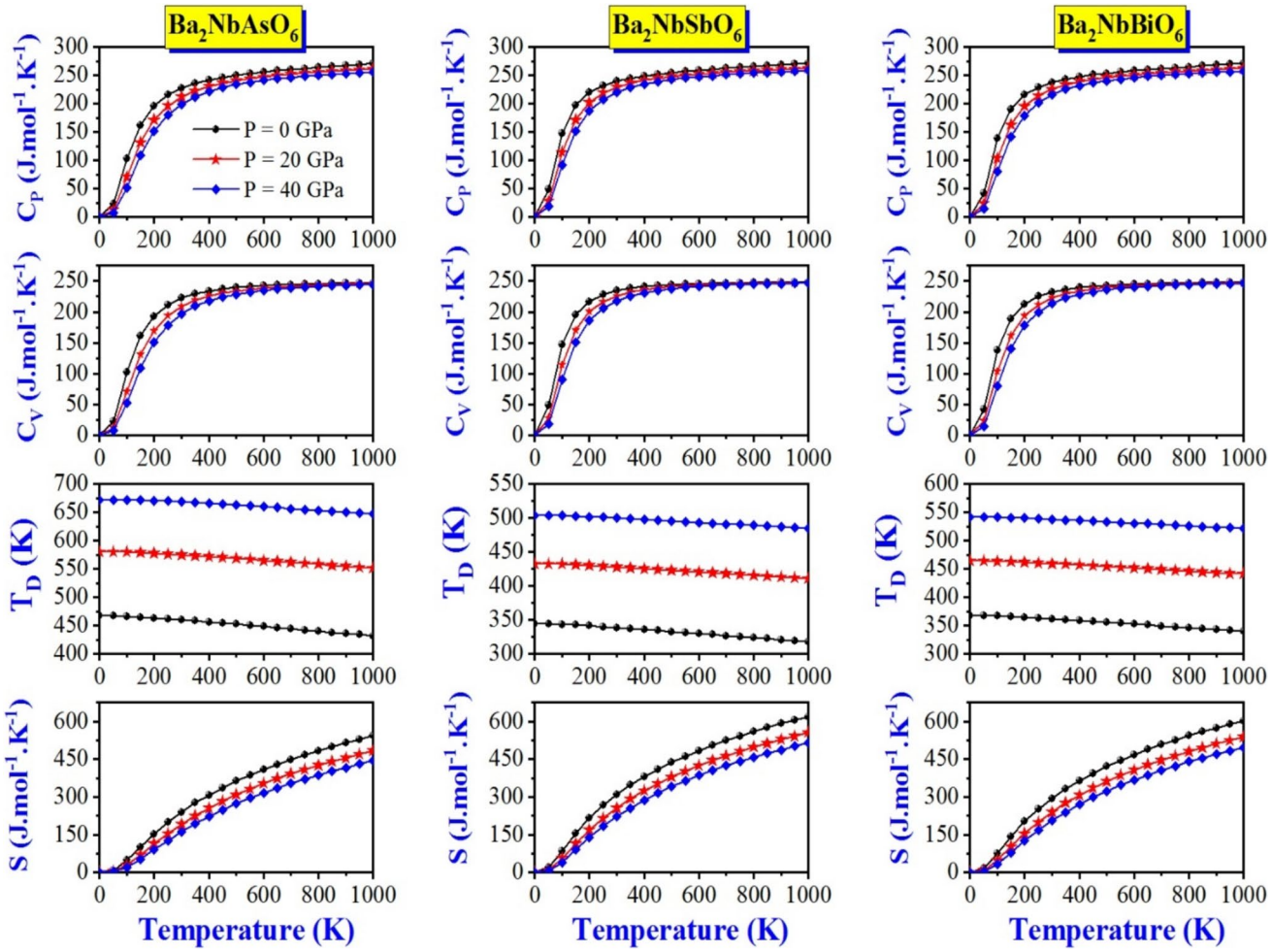

Fig. 3 Temperature dependency of the isochoric and isobaric heat capacities (C_V and C_P), Debye temperature (T_D), and thermal entropy (S) for the compounds Ba_2NbAsO_6, Ba_2NbSbO_6, and Ba_2NbBiO_6 at constant pressures of 0, 20, and 40 GPa

diminished flexibility, advantageous thermal and electrical conductivities, and lower sound insulation efficiency than Ba_2NbSbO_6 and Ba_2NbBiO_6.

Thermal entropy is an important measure that indicates the potential configurations of atoms within a substance. This thermal coefficient is closely related to many other coefficients. Figure 3 shows that as temperature increases, entropy increases due to the enhanced vibrational modes of atoms. Conversely, entropy decreases when pressure increases. The thermal entropy values of the three materials examined, especially Ba_2NbBiO_6, suggest their applicability for acoustic and thermal insulation, as their values are comparable to those of established materials such as aerogel, polyurethane, and fiberglass [46–49]. The fact that Ba_2NbSbO_6's thermal entropy is somewhat greater than that of the other two compounds proves that it is more stable under both static and dynamic conditions.

Grüneisen constant (γ) is a temperature coefficient used to describe the change in the vibrational frequencies of atoms of a material due to a change in pressure or temperature. It has a direct relationship with the volumetric expansion behavior, thermal conductivity, and dynamic stability of materials. The larger this Grüneisen constant is, the more volumetric expansion, less dynamic stability, and less thermal conductivity of the material. The Grüneisen constant values obtained for Ba_2NbAsO_6, Ba_2NbSbO_6, and Ba_2NbBiO_6 (Table 1) are somewhat close and constant with temperature variation. The moderate value of γ for the considered compounds suggests that the three compounds are thermodynamically stable with moderate thermal expansion and a low coefficient of thermal conductivity.

Figure 4 illustrates the simultaneous temperature and pressure dependencies of the bulk modulus (B), unit cell volume (V), thermal expansion coefficient (α), and lattice thermal conductivity (k_l) for Ba2 $NbAsO_6$, Ba2 $NbSbO_6$, and Ba_2NbBiO_6 across a temperature range of 0–1000 and a pressure range of 0–30 GPa. Across a temperature range of 0–1000 and a pressure range of 0–30 GPa, Figure 5 shows

Table 1 Lattice thermal conductivity (k_l, in W.m^{-1}.K^{-1}), thermal expansion coefficient (α, in 10^{-5}/K), Debye temperature (T_D, in K), isochoric and isobaric heat capacities (C_V and C_P, in J.mol^{-1}.K^{-1}), and thermal entropy (S, in J.mol^{-1}.K^{-1}), and Grüneisen parameter (γ, dimensionless) for Ba_2NbXO_6 (X = As, Sb, Bi) materials calculated at fixed temperatures T of 300, 600, and 900 K

Compounds	T	C_P	C_V	S	T_D	α	γ	k_l
Ba_2NbAsO_6	300	227.76	222.37	239.86	460.36	3.687	2.190	0.570
	600	255.88	242.60	408.63	448.48	4.164	2.190	0.264
	900	267.82	246.53	514.78	436.05	4.379	2.190	0.162
Ba_2NbSbO_6	300	240.09	234.23	310.13	338.63	3.854	2.163	0.259
	600	259.03	245.70	483.68	329.85	4.178	2.163	0.120
	900	268.88	247.85	590.65	320.84	4.357	2.163	0.074
Ba_2NbBiO_6	300	237.88	232.17	294.53	362.06	3.798	2.160	0.369
	600	258.35	245.17	467.19	352.78	4.144	2.160	0.171
	900	268.46	247.63	573.94	343.22	4.326	2.160	0.105

the simultaneous temperature and pressure dependencies of the following parameters: the isochoric and isobaric heat capacities (C_V and C_P), Debye temperature (T_D), and thermal entropy (S) for Ba_2NbAsO_6, Ba_2NbSbO_6, and Ba_2NbBiO_6.

Finally, the values of isochoric and isobaric heat capacities (C_V and C_P), entropy (S), Debye temperature (T_D), volumetric thermal expansion (α), Grüneisen parameter (γ), and lattice thermal conductivity (k_l) for the three compounds calculated at zero pressure and constant temperatures of 300, 600, and 900 K are gathered in Table 1.

3.2 Elastic Qualities

3.2.1 Single-Crystal Elastic Qualities

Elastic constants (C_{ij}) form a basic characterization of the mechanical properties of materials, which are essential to their technological applications. These parameters could be calculated trough ab initio energy-strain calculations. The elastic constants provide essential information about a wide variety of material characteristics, such as their structural stability, interatomic energy potential, forces between atoms, phase transitions properties, hardness, and stiffness [50]. For a rhombohedral system, only seven elastic constants (C_{ij}) are independent among the 21 elastic constants characterizing the elastic characteristics of a triclinic structure. Table 2 shows the calculated values of the C_{ij} parameters for the compounds considered in this work. The literature does not contain previously reported data on the C_{ij} parameters of the studied materials; therefore, our results represent the first theoretical prediction of their elastic constants.

Based on the calculated values of the C_{ij} parameters, we can observe the following:

(i) The materials considered are much more resistant to unidirectional compressive deformation than to shear deformation, as evidenced by the fact that the elastic constants C_{11} and C_{33} are significantly larger than the other elastic constants, C_{12}, C_{13}, C_{44}, and C_{15}.

(ii) C_{11} is somewhat larger than C_{33}, indicating that the materials considered will exhibit some elastic anisotropy. Furthermore, it is suggested that the material compresses somewhat more easily along the [001] direction than along the [100] direction since C_{11} and C_{33} evaluate the compressive strength along the "a" and "c" axes, respectively.

(iii) The mechanical stability of a crystal depends on its ability to resist external stresses. This stability requires that the elastic constants meet the Born-Huang requirements. The double perovskites Ba_2NbXO_6 (X = As, Sb, Bi) are mechanically stable in the rhombohedral arrangement as their C_{ij} values satisfy the mechanical stability requirements for a rhombohedral structure [51]:$(C_{11} - C_{12}) > 0$, $C_{33} > 0$, $C_{44} > 0$, $(C_{11} + C_{12}) > 0$, $\left((C_{11} + \varepsilon C_{12})C_{33} - 2C_{12}^2\right) > 0$, $\left(\left(C_{11} - C_{12}\right)C_{44} - 2C_{14}^2\right) > 0$.

3.2.2 Polycrystalline Elastic Qualities

Polycrystalline aggregates, which are collections of randomly oriented single crystals, are more common in practice than bulk single crystals. Therefore, materials in their polycrystalline state must have their mechanical and elastic properties defined. Isotropic elastic moduli, such as isotropic shear modulus (G), bulk modulus (B), Poisson's ratio (σ), and Young's modulus (E), are used to characterize the elastic properties of the polycrystalline phase of a material. According to theory, the isotropic elastic moduli given above can be obtained from the individual elastic constants C_{ij} using the Voigt-Reuss-Hill approximations [52–54]:

$$B_V = \frac{2}{9}(C_{11} + C_{12} + 2C_{13}) + C_{33}$$

$$G_V = \frac{2}{30}\left[C_{11} + C_{12} + 2(C_{33} - 2C_{13}) + 12(C_{44} + C_{66})\right]$$

$$B_R = \frac{(C_{11}+C_{12})C_{33}-2C_{13}^2}{C_{11}+C_{12}+2C_{33}-4C_{13}}\,;\; G_R = \frac{5}{2}\frac{[(C_{11}+C_{12})C_{33}-2C_{13}^2]C_{44}C_{66}}{3B_V C_{44}C_{66}+[(C_{11}+C_{12})C_{33}-2C_{13}^2](C_{44}+C_{66})}$$

$$B_H = (B_V + B_R)/2\,;\; G_H = (G_V + G_R)/2$$

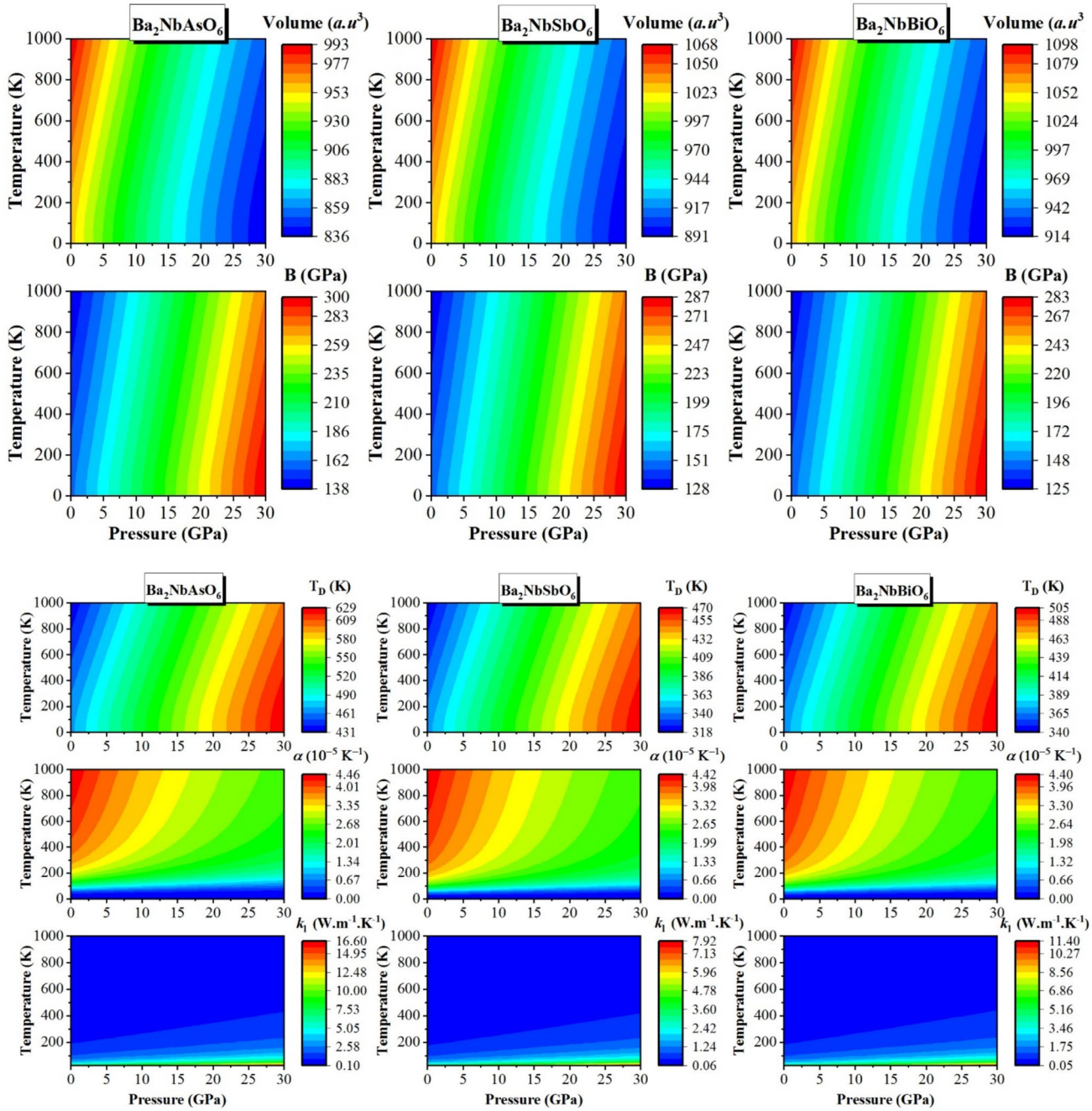

Fig. 4 Maps of the temperature and pressure simultaneous dependencies of the bulk modulus (B), unit cell volume (V), thermal expansion coefficient (α), Debye temperature (T_D), and lattice thermal conductivity (k_l) for Ba_2NbAsO_6, Ba_2NbSbO_6, and Ba_2NbBiO_6 over temperature range of 0–1000 and pressure range of 0–30 GPa

The subscripts V, R, and H refer to the employed approximation, respectively, V for Voigt, R for Reuss, and H for Hill. The Voigt approximation produces the upper bounds (B_V and G_V) of the bulk and shear moduli. The Reuss approximation yields the lower bounds (B_R and G_R). The Hill approximation yields the effective values (B_H and G_H). From B and G, the following relationships [55]:$E = \frac{9BG}{(3B+G)}$; $\sigma = \frac{(3B-2G)}{(6B+2G)}$ can be used to determine Young's modulus (E) and Poisson's ratio (σ).The predicted values of B_V, B_R, B_H, G_V, G_R, G_H, E_H, and σ_H for the explored materials are gathered in Table 3.

A number of conclusions can be drawn from the information presented in Table 3:

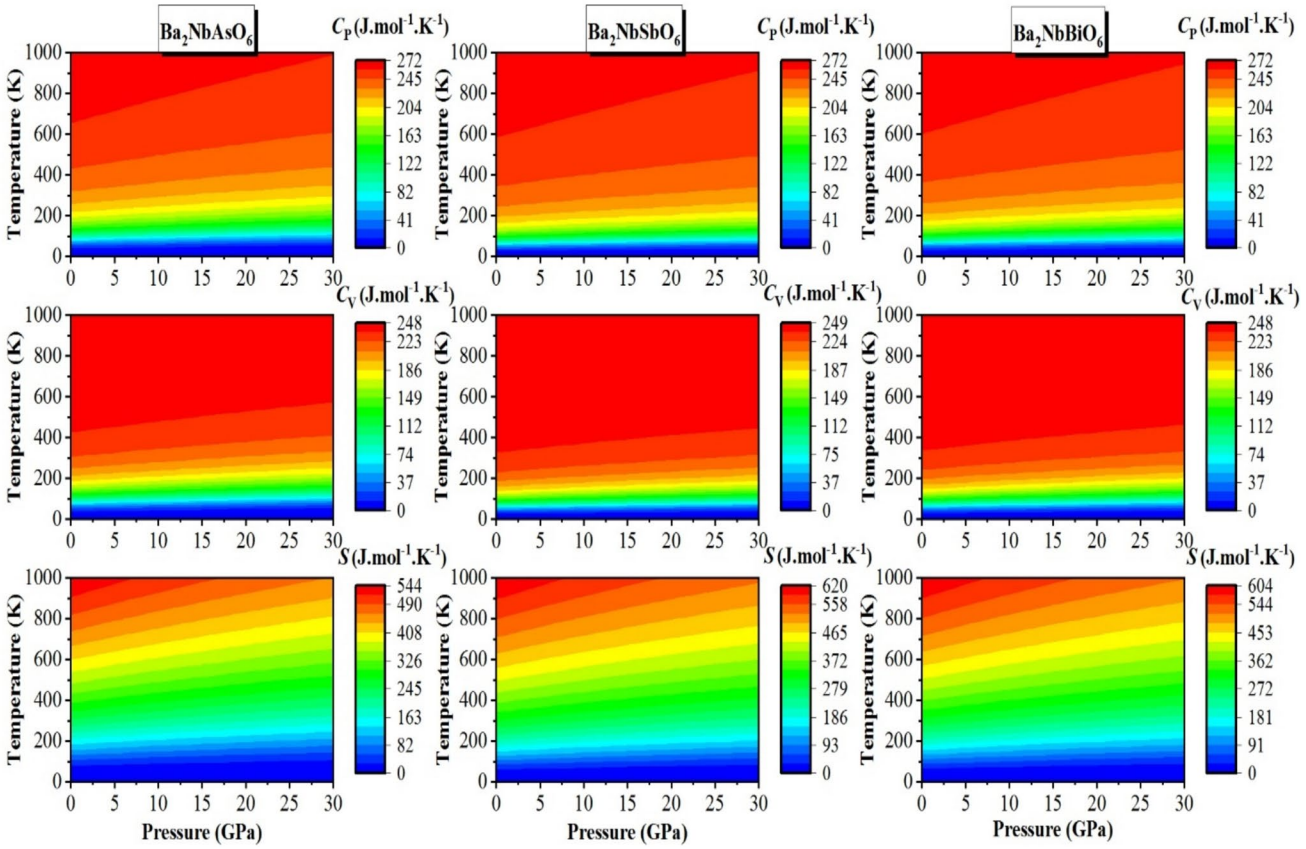

Fig. 5 Maps of the calculated temperature and pressure simultaneous dependencies of the isochoric and isobaric heat capacities (C_V and C_P) and thermal entropy (S) for the compounds Ba_2NbAsO_6, Ba_2NbSbO_6, and Ba_2NbBiO_6 over temperature range of 0–1000 and pressure range of 0–30 GPa

Table 2 The calculated values of the elastic constants (C_{ij}, in GPa) for the double perovskites Ba_2NbXO_6 (X = As, Sb, Bi) in their rhombohedral arrangement

Compound	C_{11}	C_{12}	C_{13}	C_{33}	C_{14}	C_{15}	C_{44}
Ba_2NbAsO_6	238.2	97.2	105.7	219.5	5.7	4.2	72.6
Ba_2NbSbO_6	176.8	126.3	95.7	137.4	3.2	18.7	62.0
Ba_2NbBiO_6	206.1	108.0	99.3	163.3	3.1	18.0	62.8

Table 3 The predicted Voigt, Reuss, and Hill bulk moduli values (B_V, B_R, and B_H, in GPa), shear moduli (G_R, G_V, and G_H, in GPa), Young's modulus (E_H, in GPa), and Poisson's ratio (σ_H, dimensionless) for Ba_2NbXO_6 (X = As, Sb, Bi) materials

Compounds	B_R	B_V	B_H	G_R	G_V	G_H	B_H/G_H	E_H	σ_H
Ba_2NbAsO_6	145.9	145.9	145.9	68.0	68.9	68.45	2.13	177.6	0.297
Ba_2NbSbO_6	119.6	125.2	122.4	28.3	41.4	34.82	3.51	95.4	0.370
Ba_2NbBiO_6	129.7	132.1	130.9	46.9	52.9	49.89	2.62	132.8	0.330

(i) The values of B, E, and G, which determine the resistance of solids to external deformations, decrease in the sequence $Ba_2NbAsO_6 \rightarrow Ba_2NbSbO_6 \rightarrow Ba_2NbBiO_6$. This trend indicates a decrease in the hardness of these compounds when the nature of the X atom in the compound Ba_2NbXO_6 changes from As to Sb and then to Bi.

(ii) Using Pugh's empirical criterion [56], a material can be distinguished as ductile (or brittle) if the B/G ratio is greater than (or less than) 1.75. One classifies Ba_2NbAsO_6, Ba_2NbSbO_6, and Ba_2NbBiO_6 as ductile compounds because

$B/G > 1.75$. The ductility increases in the sequence: $Ba_2NbAsO_6 \rightarrow Ba_2NbBiO_6 \rightarrow Ba_2NbSbO_6$.

(iii) Poisson's ratio (σ) provides information on the bonding properties and allows determining the stability of a crystal under shear stress. σ is about 0.1 in covalent materials and 0.25 in ionic materials [57, 58]. A strong ionic component in the bond is indicated by an σ greater than 0.25 for the materials studied.

(iv) The Debye temperature (T_D) is closely related to several thermodynamic parameters, including specific heat, thermal conductivity, thermal expansion, and melting point. T_D can be calculated using the following formulas [59]:

$$V_L = ((3B + 4G)/3\rho)^{1/2}; V_T = (G/\rho)^{1/2}; V_m = ((V_L^{-3} + 2V_T^{-3})/3)^{-1/3}; T_D = (h/k_B)((3nN_A\rho)/(4\pi M))^{1/3} V_m$$

Within this framework, V_T, V_L, and V_m denote the transverse, longitudinal, and average isotropic sound velocities, respectively. In addition, the symbol h represents Planck's constant, N_A is Avogadro's number, k_B is Boltzmann's constant, ρ is the mass density, n is the number of atoms in the molecule, M is the molecular weight, B is the bulk modulus, and G is the shear modulus. The anticipated values for mass density ρ, Debye temperature T_D, and isotropic sound velocities V_L, V_T, and V_m for Ba_2NbXO_6 (where X = As, Sb, Bi) are shown in Table 4. The sound wave velocities of these compounds at absolute zero temperature and atmospheric pressure show an increasing trend from Ba_2NbSbO_6 to Ba_2NbBiO_6 and then to Ba_2NbAsO_6, which is associated with the improvement in thermal conductivity and stiffness.

A comparison was made between the elastic characteristics of the compounds under consideration and those of other double perovskite compounds. The Young's modulus of Ba_2NbSbO_6 is lower than that of the considered two compounds and other double perovskites like Ba_2MgReO_6, Ba_2YMoO_6, Ba_2MnReO_6, Ba_2NiReO_6, and Sr_2MnReO_6 [19, 23]. This suggests that Ba_2NbSbO_6 is not as stiff as the other double perovskites. Bulk moduli values for Ba_2NbXO_6 (X = As, Sb, Bi) materials show that they are more resistant to volume change than Sr_2MnReO_6 and Ba_2MnReO_6, when subjected to hydrostatic pressure. When compared to Ba_2NbAsO_6, Ba_2NbBiO_6, Ba_2MgReO_6, Ba_2YMoO_6, Ba_2MnReO_6, Ba_2NiReO_6, and Sr_2MnReO_6, the shear deformation resistance of Ba_2NbSbO_6 is the lowest. Furthermore, the findings demonstrate that Ba_2NbSbO_6 possesses the lowest sound velocity due to its lowest values of the bulk and shear moduli, whereas Ba_2NbAsO_6 outperforms other compounds, including Ba_2MnReO_6 and Ba_2NiReO_6, in terms of average sound velocity.

3.2.3 Elastic Anisotropy Phenomenon

A material is elastically anisotropic when its elastic qualities depend on the crystal directions. While parameters such as Young's modulus, shear modulus, and Poisson's ratio are uniform in all directions in isotropic materials, anisotropic materials exhibit different elastic responses depending on the direction of applied stress. This phenomenon is important in crystals, composites, and biological tissues, where structural arrangements control mechanical behavior. Under load, elastic anisotropy can affect material stability, stress distribution, microcrack apparition, and wave propagation. Thus, it is important to characterize the elastic anisotropy of crystals. Some theoretical and experimental metrics have been developed to evaluate the extent of elastic anisotropy in crystals [60]. In this study, we used four different metrics to characterize the elastic anisotropy of the materials under study.

(i) For a rhombohedral structure, the shear anisotropy factors A_1 and A_2 are defined as follows [61]: $A_1 = 2C_{66}/(C_{11} - C_{12})$ for the {100} or {010} shear plane and $A_2 = 2C_{44}/(C_{11} + C_{33} - 2C_{13})$ for the {001} shear plane. In an isotropic crystal, A_1 and A_2 are equal to one; therefore, the extent of divergence from one indicates the degree of elastic anisotropy within the crystal. The anisotropy factors presented in Table 5 suggest that the three rhombohedral

Table 5 Numerical evaluations of the shear anisotropic factors (A_1, A_2), percentages of anisotropy in compressibility (A_C) and shear (A_S), and universal elastic anisotropy factor (A^U) for the double perovskites Ba_2NbXO_6 (X = As, Sb, Bi) in their rhombohedral arrangement

Compound	A_1	A_2	A_C (%)	A_S (%)	A^U
Ba_2NbAsO_6	1	0.092	0.023	0.70	0.070
Ba_2NbSbO_6	1	0.104	2.27	18.88	2.374
Ba_2NbBiO_6	1	0.072	0.92	5.96	0.652

Table 4 The calculated molecular weight (M, in g.mol^{-1}), density of mass (ρ, in g.cm^{-3}), longitudinal, transverse, and average sound velocities (V_L, V_T, and V_m, in m.s^{-1}), and Debye temperatures (T_D, in K) for the Ba_2NbXO_6 (X = As, Sb, Bi) polycrystals

Compound	M	ρ	V_l	V_t	V_m	T_D
Ba_2NbAsO_6	538.48	6.35	6109.7	3282.4	3665.0	452.0
Ba_2NbSbO_6	585.32	6.43	5123.5	2327.0	2623.4	315.9
Ba_2NbBiO_6	672.54	7.17	5245.5	2637.0	2957.3	352.7

Ba_2NbXO_6 (X = As, Sb, Bi) exhibit little anisotropy on the {001} plane, while demonstrating greater isotropy on the {100} or {010} planes.

(ii) The percentages of anisotropy in compressibility (A_C) and in shear (A_S) are defined as follows [62]:

$A_C = \frac{((B_V - B_R))}{((B_V + B_R))} \times 100$, and $A_S = \frac{(G_V - G_R)}{(G_V + G_R)} \times 100$ are usually used to the elastic anisotropy in compression and shear of crystals. Here, B and G are the bulk and shear moduli, respectively, and the indices V and R represent the Voigt and Reuss limits. The values of A_C and A_S can vary from zero to 100%. The values of A_C and A_S show that the shear anisotropy is relatively more pronounced than the elastic compression anisotropy for the three compounds.

(iii) A third approach to quantify elastic anisotropy is the universal index [54] $A^U (A^U = 5\frac{G_V}{G_R} + \frac{B_V}{B_R} - 6)$, which incorporates both compression and shear contributions. In isotropic crystals, A^U is zero, and consequently, the magnitude of divergence of A^U from zero indicates the level of elastic anisotropy. The calculated values of A^U further suggest the existence of elastic anisotropy in the analyzed crystals.

(iv) Three-dimensional (3D) and two-dimensional (2D) representations of the crystal direction dependence of a crystal's elastic modulus are widely used to visualize the extent of elastic anisotropy in crystals. The dependence Young's modulus (E) on the crystal direction in a trigonal system is expressed in the spherical coordinate system as follows [55]:

$$\frac{1}{E} = (1 - l_3^2)S_{11} + l_3^4 S_{33} + (2S13 + S44)l_3^2(1 - l_3^2) + 2S_{14}l_2l_3(3l_1^2 - l_2^2)$$

.

In this context, the S_{ij} parameters are the components of the compliance matrix, and l_1, l_2, and l_3 are the direction cosines of a direction in the spherical coordinates. An isotropic elastic modulus has a uniform magnitude in all directions of the crystal. Therefore, in a 3D representation, it is depicted as a closed surface of an ideal spherical shape, and in a 2D representation, it is illustrated as a perfect circular shape. The degree of anisotropy of the represented elastic modulus correlates with the extent to which the configuration of this closed surface deviates from a spherical shape. Figure 4 illustrates the 3D representations of Young's modulus (E), as well as its 2D representations in the (001), (010), and (001) crystal planes for the three materials analyzed. The 3D representations (2D representations) of Young's modulus E diverge considerably from the spherical shape (circular form). This means that this property is considerably anisotropic for all three substances examined. The minimum values of E (E_{min}) are 153 GPa for Ba_2NbAsO_6, 55 GPa for Ba_2NbSbO_6, and 101 GPa for Ba_2NbBiO_6, and the maximum values of E (E_{max}) are 200 GPa for Ba_2NbAsO_6, 162 GPa for Ba_2NbSbO_6, and 191 GPa for Ba_2NbBiO_6. There is a large difference between the highest value of E (E_{max}) and the lowest value of E (E_{min}), indicating the considerable anisotropy of this feature.

From Fig. 6, it is worth noting the significant anisotropy of the Young's modulus in Ba_2NbSbO_6 and Ba_2NbBiO_6 in comparison to Ba_2NbAsO_6. Below is a breakdown of potential reasons for this difference in anisotropy among the considered materials:

1. Atomic size and ionic radius differences:
   - As, Sb, and Bi belong to the same group (Group 15) but have increasing ionic radii (As^{3+}≈0.59 A°, Sb^{3+}≈0.84 A°, Bi^{3+}≈1.03 A°).
   - Substituting As with larger Sb or Bi ions disrupts lattice symmetry, causing anisotropic strain in the crystal structure. This strain likely manifest as directional differences in bond strength or coordination geometry, resulting in pronounced anisotropy in the elastic moduli.
2. Bonding and electronic structure:
   - Heavier elements such as Bi (and, to a lesser extent, Sb) display relativistic effects that distort bonding character. This may lead to directional variations in covalency or ionicity, affecting stiffness differently along crystal axes.
   - The electronic configurations of Sb and Bi (compared to As) might also induce local structural distortions that further enhance anisotropy.

3.3 Thermoelectric Properties

Temperature influences not only atomic vibrations but also the mobility of charge carriers, including electrons and holes. The semi-classical Boltzmann model allows us to estimate this effect by calculating the relationship between temperature and the Seebeck coefficient (S) and thermal and electrical conductivities (k_e, σ).

Figures 7, 8, and 9 illustrate the correlation between the Seebeck coefficient (S)—which characterizes the potential difference across a material subjected to a temperature gradient—and the concentrations of holes and electrons along the three principal crystallographic axes, namely the [100], [010], and [001] crystal directions, at constant temperatures of 300, 600, and 900 K for Ba_2NbAsO_6, Ba_2NbAsO_6, and Ba_2NbAsO_6. The Seebeck coefficient values for electrons exceed those for holes in all three considered substances. In all three considered compounds, the Seebeck coefficient values for electrons and holes increase with increasing temperature and decrease with increasing charge carrier concentration. It is worth noting that the Seebeck coefficient

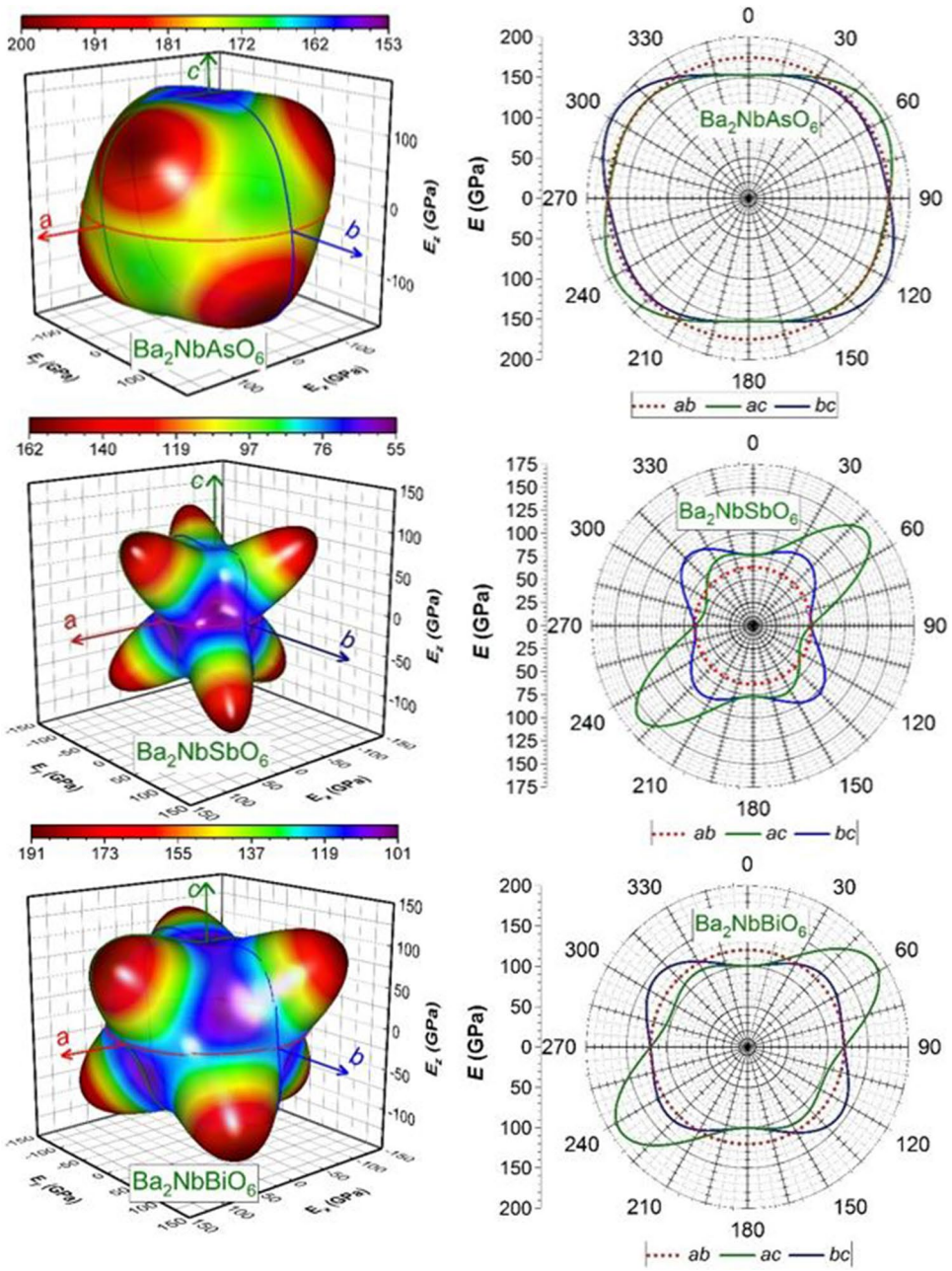

Fig. 6 3D visualizations of Young's modulus, as well as its 2D visualization in the *ab*, *ac*, and *bc* planes for Ba_2NbXO_6 (*X* = As, Sb, Bi) materials

values in the three crystallographic directions are close when calculated at the same temperature and concentration. At a temperature of 300 K and an electron concentration of 10^{17} cm^{-3}, the value of the Seebeck coefficient for Ba_2NbAsO_6 is about 1.0 mV/K and about 0.8 mV/K for Ba_2NbBiO_6 and Ba_2NbSbO_6.

Figures 7, 8, and 9 show that as the concentration of charge carriers increases, both the electronic thermal conductivity (k_e) and electrical conductivity (σ) increase. The electronic thermal conductivity increases as the temperature increases, but the electrical conductivity decreases as the temperature increases. Holes play a more important role in thermal and electrical conductivities than electrons. In addition, the thermal and electrical conductivities of electrons as well as those of holes are almost the same in the three crystallographic directions [100], [001], and [010], highlighting the isotropy of these features. Figures 7, 8, and 9 show that Ba_2NbBiO_6 and Ba_2NbSbO_6 have comparable thermal and electrical conductivities, which somewhat exceed those of Ba_2NbAsO_6.

To compute the figure of merit (ZT) expressed as $ZT = \sigma ST/(k_e + k_l)$ along the [100], [010], and [001] crystal orientations, we initially assessed the temperature dependence of lattice thermal conductivity (k_L) in these three

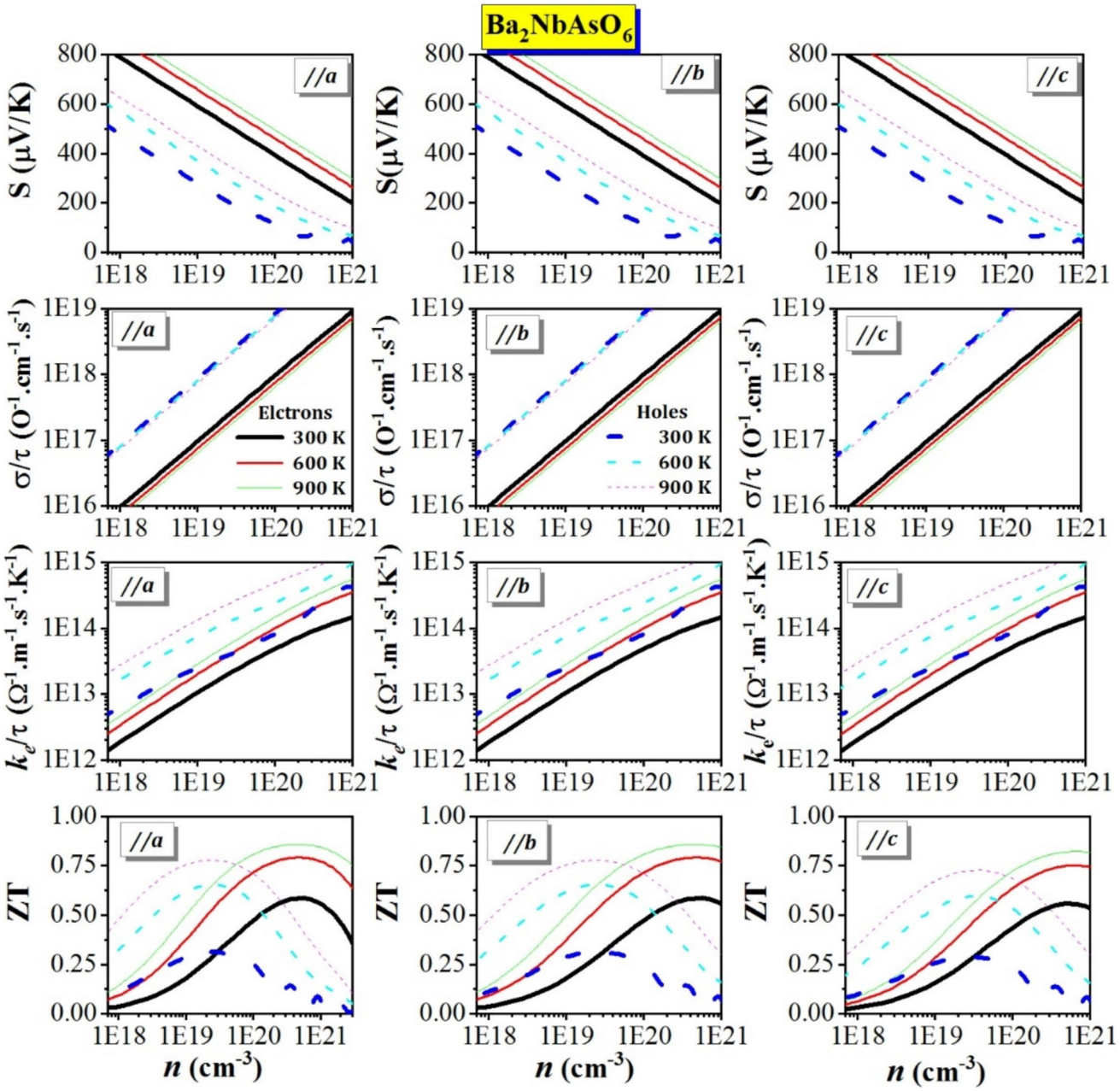

Fig. 7 Seebeck coefficient (S), electronic thermal conductivity (k_e), electrical conductivity (σ), and figure of merit (ZT) as a function of charge carrier concentration (n) at fixed temperatures of 300, 600, and 900 K for Ba_2NbAsO_6. τ is the relaxation time

crystalline directions as shown in Fig. 10. To achieve this objective, we utilized the phono3py software, which operates on the Boltzmann transport equation (BTE) principles. Figure 5 illustrates the variation of k_l for the compounds Ba_2NbAsO_6, Ba_2NbSbO_6, and Ba_2NbBiO_6 with temperature in the range of 300–1000 K along the [100], [010], and [001] crystallographic directions. Notably, the lattice thermal conductivity rapidly declines with increasing temperatures across the three crystallographic orientations examined for the three substances. The results indicate that the lattice thermal conductivity in the [001] direction surpasses that of the other two orientations.

Figures 7, 8, and 9 show the variations of ZT along the [100], [010], and [001] crystal orientations as a function of the charge carrier concentration at fixed temperatures of 300, 600, and 900 K for the compounds Ba_2NbAsO_6, Ba_2NbBiO_6, and Ba_2NbSbO_6. We must mention that we established the relaxation time (τ) at a standard value of 10^{-14} s. Some conclusions can be drawn from Figs. 7, 8, and 9: for identical charge carrier concentration and temperature, the ZT figures of merit along

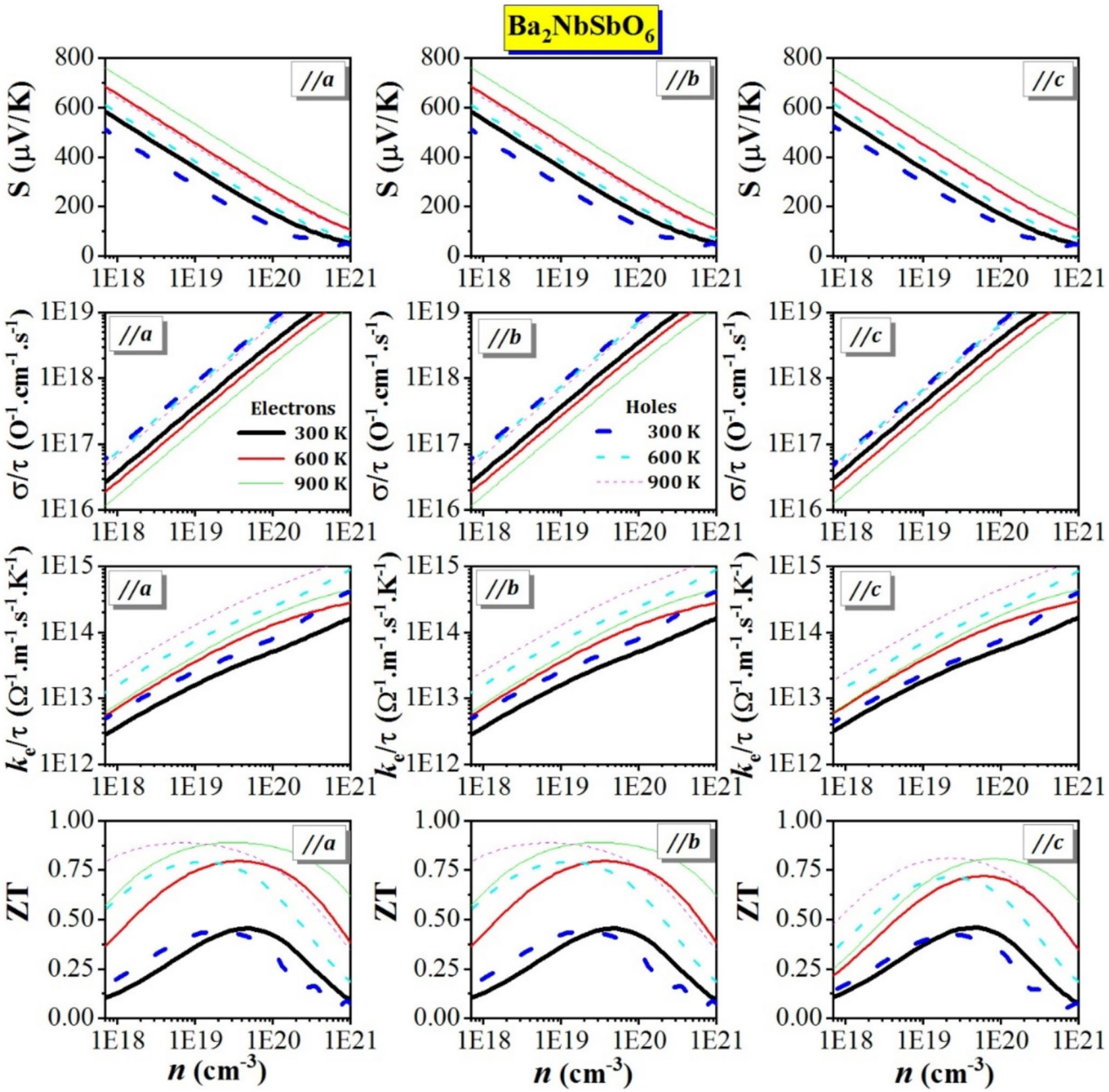

Fig. 8 Seebeck coefficient (S), electronic thermal conductivity (k_e), electrical conductivity (σ), and figure of merit (ZT) as a function of charge carrier concentration (n) at fixed temperatures of at 300, 600, and 900 K for Ba_2NbSbO_6. τ is the relaxation time

the [100] and [010] crystal orientations are somewhat more significant than along the [001] direction, suggesting a weak anisotropy of this property. The maximum ZT value reached at a fixed temperature for electrons is more significant than that for holes in Ba_2NbAsO_6 and Ba_2NbSbO_6, indicating that n-type doping is more favorable for thermoelectric efficiency than p-type doping in these compounds. The compounds Ba_2NbAsO_6 and Ba_2NbBiO_6 have a figure of merit slightly lower than that of Ba_2NbAsO_6 when measured at the same temperature and charge carrier concentration. In Ba_2NbBiO_6, the maximum value of ZT at a fixed temperature for electrons is nearly equal to that for holes. ZT increases with rising temperature for a fixed charge carrier concentration. Conversely, at a constant temperature, ZT rises with increasing charge carrier concentration until it reaches a maximum and begins declining. In Ba_2NbAsO_6, ZT attains a maximum value of approximately 0.87 for an electron concentration of approximately 5×10^{20} cm^{-3} at 900 K along the [100] and [010] directions and approximately 0.83 for an electron concentration of approximately 8×10^{20} cm^{-3} at 900 K along the [001]

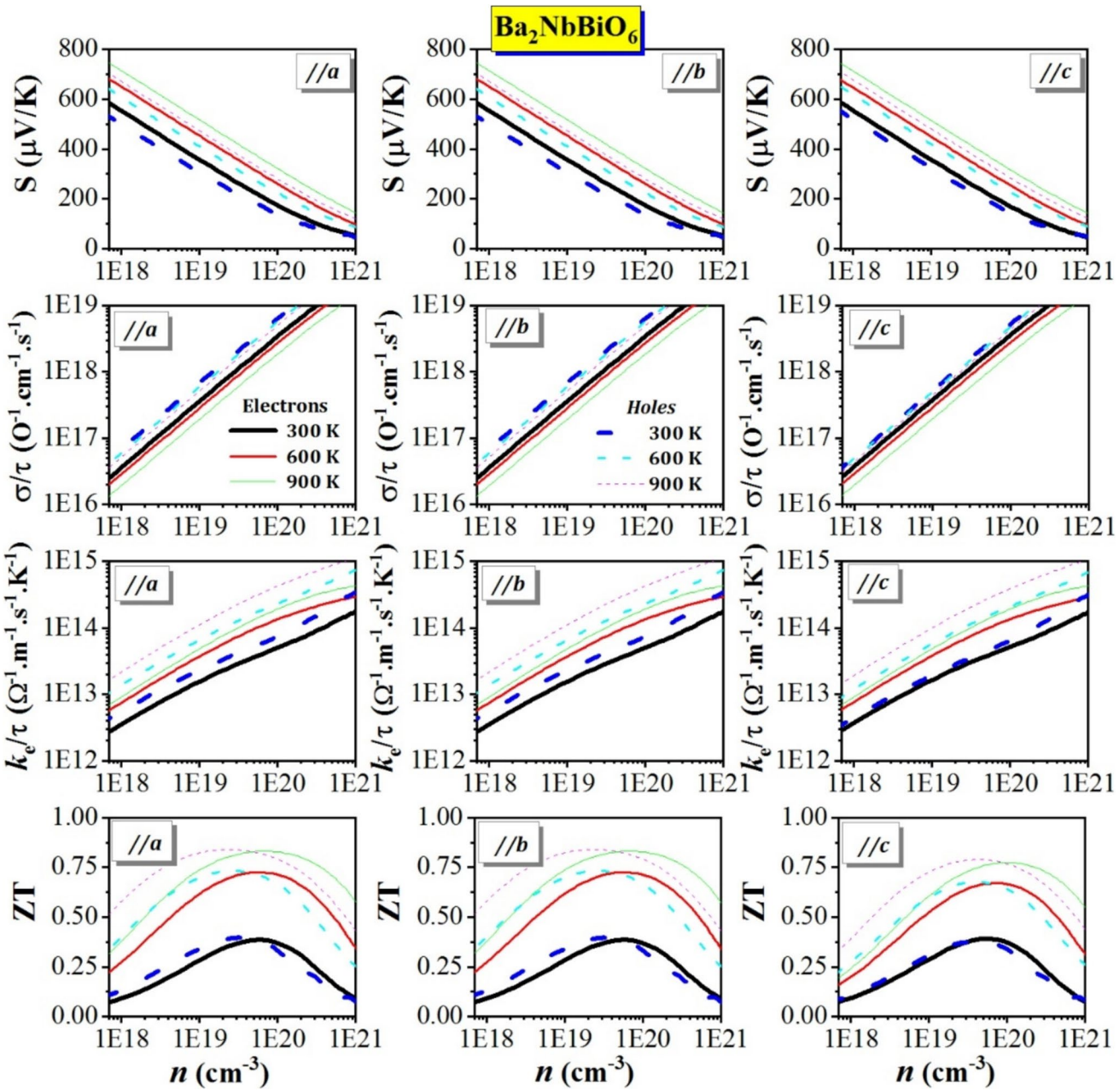

Fig. 9 Seebeck coefficient (S), electronic thermal conductivity (k_e), electrical conductivity (σ), and figure of merit (ZT) as a function of charge carrier concentration (n) at fixed temperatures of at 300, 600, and 900 K for of Ba_2NbBiO_6. τ is the relaxation time

direction. In Ba_2NbSbO_6, ZT achieves a maximum of about 0.89 for an electron concentration of around 3.5×10^{19} cm^{-3} at 900 K along the [100] and [010] directions, and about 0.81 for an electron concentration of around 8×10^{19} cm^{-3} at 900 K along the [001] direction. In Ba_2NbBiO_6, ZT achieves a maximum value of 0.83 for an electron concentration of about 8×10^{19} cm^{-3} at 900 K along the [100] and [010] directions and approximately 0.8 for an electron concentration of about 1×10^{20} cm^{-3} at 900 K along the [001] direction.

4 Conclusion

We have comprehensively analyzed the elastic, thermodynamic, and thermoelectric characteristics of Ba_2NbBO_6 (B = As, Sb, and Bi) double perovskites in rhombohedral configuration using the strain-energy technique, the quasi-harmonic Debye model, and the semi classical Boltzmann transport theory, respectively, combined with first-principles PP-PW and FP-LAPW methods. The main conclusions are as follows:

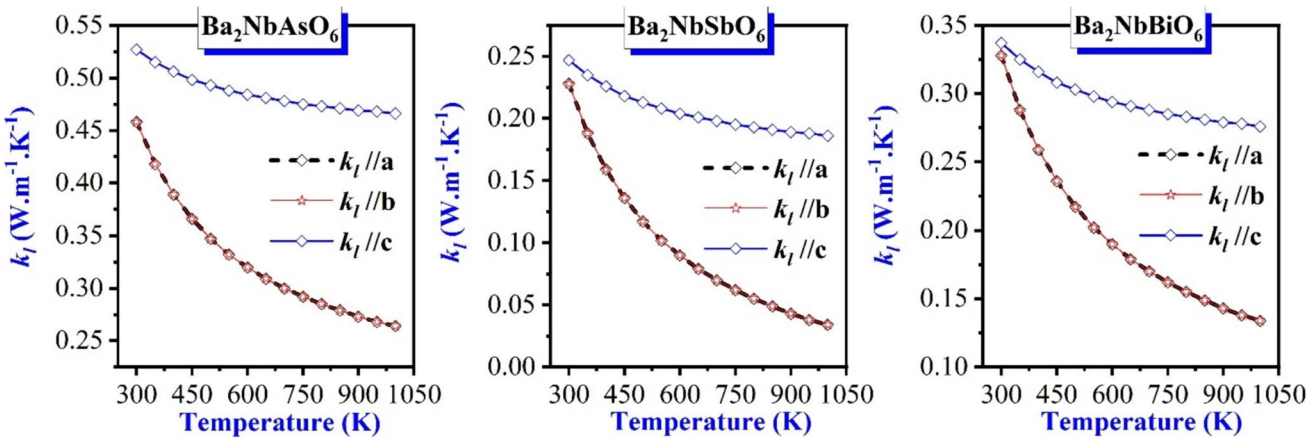

Fig. 10 Temperature dependency of lattice thermal conductivity along the [100], [010], and [001] crystal orientations for the compounds Ba_2NbAsO_6, Ba_2NbSbO_6, and Ba_2NbBiO_6

1. Monocrystalline and polycrystalline elastic moduli and associated characteristics were predicted. Monocrystalline elastic constants support the mechanical stability of the materials considered. All three compounds exhibit moderate hardness, decreasing slightly from Ba_2NbBiO_6 to Ba_2NbSbO_6 and then to Ba_2NbAsO_6. All three materials studied exhibit significant elastic anisotropy.
2. Maps visualizing the temperature and pressure dependencies of some macroscopic physical parameters, including unit cell volume, bulk modulus, volumetric thermal expansion, isochoric and isobaric heat capacities, and Debye temperature, have been predicted over wide temperature ranges from 0 to 1000 K and pressure ranges from 0 to 30 GPa.
3. The low thermal conductivity at room temperature, moderate coefficient of thermal expansion, and Grüneisen constant values of the three compounds show that they are suitable for use as thermal insulators.
4. A figure of merit exceeding 0.8 over a large charge carrier concentration, a Seebeck coefficient greater than 0.9 mV/K, and high electrical conductivity make Ba_2NbAsO_6, Ba_2NbBiO_6, and Ba_2NbSbO_6 compounds suitable potential candidates for use in heat-to-electricity conversion.

Acknowledgements Y. Al-Douri would like to acknowledge Al-Bayan University for fruitful support.

Author Contribution Saber Saad Essaoud: Conceptualization, Methodology, Writing and Investigation. Formal analysis Missoum Radjai: Methodology, Writing and Investigation. Formal analysis. Abdelmadjid Bouhemadou: software, Visualization. Writing and Investigation. Formal analysis. Mohammed Elamin Ketfi: Verification. Supervision. Verification. Djamel Allali: Verification. Supervision. Verification. Y.Al-Douri: Verification. Supervision. Verification. R.Khenata: Verification. Supervision. Verification.

Data Availability No datasets were generated or analysed during the current study.

Declarations

Competing interests The authors declare no competing interests.

References

1. Khan, M.A.I., Khan, M.I., Kazim, A.H., Shabir, A., Riaz, F., Mustafa, N., Javed, H., Raza, A., Hussain, M., Salman, C.A.: An experimental and comparative performance evaluation of a hybrid photovoltaic-thermoelectric system. Front. Energy Res. **9**, 722514 (2021)
2. Ahadi, S., Hoseini, H.R., Faez, R.: Using of thermoelectric devices in photovoltaic cells in order to increase efficiency. Indian J. Sci. Res. **2**, 20–26 (2014)
3. Sahin, A.Z., Ismaila, K.G., Yilbas, B.S., Al-Sharafi, A.: A review on the performance of photovoltaic/thermoelectric hybrid generators. Int. J. Energy Res. **44**, 3365–3394 (2020). https://doi.org/10.1002/er.5139
4. Shakouri, A.: Recent developments in semiconductor thermoelectric physics and materials. Annu. Rev. Mater. Res. **41**, 399–431 (2011). https://doi.org/10.1146/annurev-matsci-062910-100445
5. Cui, T., Xuan, Y., Yin, E., Li, Q., Li, D.: Experimental investigation on potential of a concentrated photovoltaic-thermoelectric system with phase change materials. Energy. **122**, 94–102 (2017)
6. He, W., Zhou, J., Hou, J., Chen, C., Ji, J.: Theoretical and experimental investigation on a thermoelectric cooling and heating system driven by solar. Appl. Energy. **107**, 89–97 (2013)
7. Parida, B.N., Panda, N., Padhee, R., Parida, R.K.: Ferroelectric and optical behavior of $Pb_{0.5}$ $Ba_{1.5}$ $BiNbO_6$ double perovskite.

Ferroelectrics. **540**, 18–28 (2019). https://doi.org/10.1080/00150193.2019.1611101
8. Wang, K., He, Y., Zhang, M., Shi, J., Cai, W.: Promising lead-free double-perovskite photovoltaic materials $Cs_2MM'Br_6$ (M = Cu, Ag, and Au; M′ = Ga, In, Sb, and Bi) with an ideal band gap and high power conversion efficiency. J. Phys. Chem. C. **125**, 21160–21168 (2021). https://doi.org/10.1021/acs.jpcc.1c05699
9. Mateo, D., Cerrillo, J.L., Durini, S., Gascon, J.: Fundamentals and applications of photo-thermal catalysis. Chem. Soc. Rev. **51**, 1547–1547 (2022)
10. Matli, P.R., Mohamed, A.M.A., Rajuru, R.R.: Microwave fast sintering of double perovskite ceramic materials. Adv. Ceram. Process, (2015). https://doi.org/10.5772/61026
11. Lu, Y., Dai, T., Lu, C., Cao, C., Zhang, W., Xu, W., Min, H., Yang, X.: Fabrication of doped SmBaCo2O5+δ double perovskites for enhanced solar-driven interfacial evaporation. Ceram. Int. **45**, 24903–24908 (2019). https://doi.org/10.1016/j.ceramint.2019.08.131
12. Ishfaq, M., Yaseen, M., Shukrullah, S., Noreen, S.: Optoelectronic and thermoelectric transport phenomena in Sr2LaTaO6 and Sr2LuTaO6 double perovskites. Mater. Chem. Phys. **313**, 128728 (2024). https://doi.org/10.1016/j.matchemphys.2023.128728
13. Ishfaq, M., Aldaghfag, S.A., Zahid, M., Yaseen, M., Awwad, N.S.: DFT investigation of optoelectronic and thermoelectric features of Ba2Ce(Sn, Pt)O6 double perovskites. Mater. Chem. Phys. **321**, 129493 (2024). https://doi.org/10.1016/j.matchemphys.2024.129493
14. Saad Essaoud, S., Ketfi, M.E., Al Azar, S., Al-Reyahi, A.Y., Mufleh, A.: Computational study of structural parameters, magnetic properties, half metallicity, and linear optical characteristics of transition-metal oxide double perovskites: Ba2MnReO6, Ba2NiReO6, and Sr2MnReO6. Indian J. Phys. (2024). https://doi.org/10.1007/s12648-024-03264-7
15. Belhachi, S., Al-Qaisi, S., Samah, S., Rached, H., Zaman, A., Alrebdi, T.A., Boutramine, A., Erum, N., Ahmed, R., Verma, A.S.: DFT analysis of Ba2NbRhO6: a promising double perovskite for sustainable energy applications. J. Inorg. Organomet. Polym. Mater. (2024). https://doi.org/10.1007/s10904-024-03336-5
16. Ahmad Dar, S., Srivastava, V., Kumar Sakalle, U., Parey, V., Pagare, G.: A combined DFT, DFT + U and mBJ investigation on electronic structure, magnetic, mechanical and thermodynamics of double perovskite Ba2ZnOsO6. Mater. Sci. Eng. B. **236–237**, 217–224 (2018). https://doi.org/10.1016/j.mseb.2018.12.007
17. Azeem, W., Hussain, S., Shahzad, M.K., Azad, F., Khan, G., Tirth, V., Alqahtani, H., Algahtani, A., Al-Mughanam, T., Wong, Y.H.: Computational insights of double perovskite X2CaCdH6 (X = Rb and Cs) hydride materials for hydrogen storage applications: a DFT analysis. Int. J. Hydrog. Energy. **79**, 514–524 (2024). https://doi.org/10.1016/j.ijhydene.2024.07.044
18. Annie Abraham, J., Behera, D., Kumari, K., Srivastava, A., Sharma, R., Kumar Mukherjee, S.: A comprehensive DFT analysis on structural, electronic, optical, thermoelectric, SLME properties of new double perovskite oxide Pb2ScBiO6. Chem. Phys. Lett. **806**, 139987 (2022). https://doi.org/10.1016/j.cplett.2022.139987
19. Ketfi, M.E., Essaoud, S.S., Al Azar, S.M., Al-Reyahi, A.Y., Mousa, A.A., Al-Aqtash, N.: Mechanical, magneto-electronic and thermoelectric properties of Ba2MgReO6 and Ba2YMoO6 based cubic double perovskites: an ab initio study. Phys. Scr. **99**, 015908 (2023). https://doi.org/10.1088/1402-4896/ad1021
20. Sâad Essaoud, S., Al Azar, S.M., Mousa, A.A., Al-Reyahi, A.Y.: DFT-based investigation of electronic-structure, magnetic and thermoelectric properties of Dy2CoMnO6 double perovskite. Phys. Scr. (2023). https://doi.org/10.1088/1402-4896/acdd2c
21. Alotaibi, N.H., Mustafa, G.M., Kattan, N.A., Mahmood, Q., Albalawi, H., Morsi, M., Somaily, H.H., Hafez, M.A., Mahmoud, H.I., Amin, M.A.: DFT study of double perovskites Cs2AgBiX6 (X = Cl, Br): an alternative of hybrid perovskites. J. Solid State Chem. **313**, 123353 (2022). https://doi.org/10.1016/j.jssc.2022.123353
22. Sivasamy, R., Venugopal, P., Espinoza-González, R.: Structure, electronic structure, optical and magnetic studies of double perovskite Gd2MnFeO6 nanoparticles: first principle and experimental studies. Mater. Today Commun. **25**, 101603 (2020). https://doi.org/10.1016/j.mtcomm.2020.101603
23. Saad Essaoud, S., Elamin Ketfi, M., Al-Reyahi, A.Y., Al Azar, S.M.: Computational prediction of thermo-elastic and charge carriers transport properties of Ba2MnReO6, Ba2NiReO6, and Sr2MnReO6 double perovskite compounds. Chem. Phys. Lett. **857**, 141694 (2024). https://doi.org/10.1016/j.cplett.2024.141694
24. Ketfi, M.E., Essaoud, S.S., Al-Reyahi, A.Y., Al Azar, S.M.: Structural, electronic, optical, and magnetic properties of NbFePb2O6 ferromagnetic semiconductor double perovskite compound. Chem. Phys. Lett. 142022 (2025). https://doi.org/10.1016/j.cplett.2025.142022
25. Giannozzi, P., Baroni, S., Bonini, N., Calandra, M., Car, R., Cavazzoni, C., Ceresoli, D., Chiarotti, G.L., Cococcioni, M., Dabo, I.: QUANTUM ESPRESSO: a modular and open-source software project for quantum simulations of materials. J. Phys. Condens. Matter. **21**, 395502 (2009)
26. Perdew, J.P., Ruzsinszky, A., Csonka, G.I., Vydrov, O.A., Scuseria, G.E., Constantin, L.A., Zhou, X., Burke, K.: Restoring the density-gradient expansion for exchange in solids and surfaces. Phys. Rev. Lett. **100**, 136406 (2008)
27. Blaha, P., Schwarz, K., Tran, F., Laskowski, R., Madsen, G.K., Marks, L.D.: WIEN2k: an APW+ lo program for calculating the properties of solids. J. Chem. Phys. **152**, 074101 (2020)
28. Essaoud, S.S., Radjai, M., Bouhemadou, A., Ketfi, M.E., Allali, D.: Fundamental physical features of the rhombohedral structure of double perovskite compounds Ba2NbBO6 (B= As, Sb, and Bi). Chem. Phys. **591**, 112578 (2025)
29. Becke, A.D., Johnson, E.R.: A simple effective potential for exchange. Am. Inst. Phys. (2006). https://doi.org/10.1063/1.2213970
30. Togo, A., Chaput, L., Tanaka, I.: Distributions of phonon lifetimes in Brillouin zones. Phys. Rev. B. **91**, 094306 (2015). https://doi.org/10.1103/PhysRevB.91.094306
31. Madsen, G.K., Carrete, J., Verstraete, M.J.: BoltzTraP2, a program for interpolating band structures and calculating semi-classical transport coefficients. Comput. Phys. Commun. **231**, 140–145 (2018)
32. Goumri-Said, S.: Probing optoelectronic and thermoelectric properties of lead-free perovskite SnTiO3: HSE06 and Boltzmann transport calculations. Crystals. 12, (2022). https://doi.org/10.3390/cryst12091317
33. Chen, W., Pöhls, J.-H., Hautier, G., Broberg, D., Bajaj, S., Aydemir, U., Gibbs, Z.M., Zhu, H., Asta, M., Snyder, G.J., Meredig, B., White, M.A., Persson, K., Jain, A.: Understanding thermoelectric properties from high-throughput calculations: trends, insights, and comparisons with experiment. J. Mater. Chem. C. **4**, 4414–4426 (2016). https://doi.org/10.1039/C5TC04339E
34. Bhattacharya, S., Madsen, G.K.H.: A novel p-type half-Heusler from high-throughput transport and defect calculations. J. Mater. Chem. C. **4**, 11261–11268 (2016). https://doi.org/10.1039/C6TC04259G
35. Ryu, B., Oh, M.-W.: Computational simulations of thermoelectric transport properties. J. Korean Ceram. Soc. **53**, 273–281 (2016)
36. Faghaninia, A., Yu, G., Aydemir, U., Wood, M., Chen, W., Rignanese, G.-M., Snyder, G.J., Hautier, G., Jain, A.: A computational

assessment of the electronic, thermoelectric, and defect properties of bournonite (CuPbSbS3) and related substitutions. Phys. Chem. Chem. Phys. **19**, 6743–6756 (2017). https://doi.org/10.1039/C7CP00437K
37. A. Otero-de-la-Roza, D. Abbasi-Pérez, V.L.: Gibbs2: a new version of the quasiharmonic model code. II. Models for solid-state thermodynamics, features and implementation. Comput. Phys. Commun. **182**(10), 2232–2248 (2011)
38. A. Otero-de-la-Roza, V.L.: Gibbs2: a new version of the quasiharmonic model code. I. Robust treatment of the static data,. Comput. Phys. Commun. **182**(8), 1708–1720 (2011)
39. Momma, K., Izumi, F.: ıt VESTA3 for three-dimensional visualization of crystal, volumetric and morphology data. J. Appl. Crystallogr. **44**, 1272–1276 (2011). https://doi.org/10.1107/S0021889811038970
40. Patwe, S.J., Achary, S.N., Mathews, M.D., Tyagi, A.K.: Synthesis, phase transition and thermal expansion studies on M2MgWO6 (M=Ba2+ and Sr2+) double perovskites. J. Alloys Compd. **390**, 100–105 (2005). https://doi.org/10.1016/j.jallcom.2004.05.093
41. Slack, G.A.: Nonmetallic crystals with high thermal conductivity. J. Phys. Chem. Solids. **34**, 321–335 (1973)
42. Dulong, P.L., Petit, A.-T.: Recherches sur quelques points importans de la theorie de la chaleur. Annales de Chimie et de Physique. **10**, 395–413 (1819)
43. Rahimi-Ahar, Z., Ahar, L.R.: Thermal, optical, mechanical, dielectric, and electrical properties of nanocomposites. Eur. Polym. J. 113337 (2024). https://doi.org/10.1016/j.eurpolymj.2024.113337
44. Dai, R., Cheng, R., Wang, J., Zhang, C., Li, C., Wang, H., Wang, X., Zhou, Y.: Tunnel-structured willemite Zn2SiO4: electronic structure, elastic, and thermal properties. J. Adv. Ceram. **11**, 1249–1262 (2022). https://doi.org/10.1007/s40145-022-0607-1
45. Kumar, A., Jain, A., Yusuf, S., Dhaka, R.: Observation of anisotropic thermal expansion and the Jahn-Teller effect in double perovskites Sr2–x La x CoNbO6 using neutron diffraction. J. Phys. Chem. Lett. **13**, 3023–3031 (2022)
46. Ijjada, N., Nayaka, R.R.: Review on properties of some thermal insulating materials providing more comfort in the building. Mater. Today Proc. **58**, 1354–1359 (2022)
47. Dourbash, A., Buratti, C., Belloni, E., Motahari, S.: Preparation and characterization of polyurethane/silica aerogel nanocomposite materials. J. Appl. Polym. Sci. 134, app.44521 (2017). https://doi.org/10.1002/app.44521
48. Arenas, J.P., Crocker, M.J.: Recent trends in porous sound-absorbing materials. Sound Vib. **44**, 12–18 (2010)
49. Cuce, E., Cuce, P.M., Wood, C.J., Riffat, S.B.: Toward aerogel based thermal superinsulation in buildings: a comprehensive review. Renew. Sustain. Energy Rev. **34**, 273–299 (2014)
50. Radjai, M., Bouhemadou, A.: Physical properties of BaRu2X2 (X= P, As) superconducting compound sunder pressure effects: ab initio study. Phys. C Supercond. Its Appl. **604**, 1354176 (2023)
51. Wang, J.J., Meng, F.Y., Ma, X.Q., Xu, M.X., Chen, L.Q.: Lattice, elastic, polarization, and electrostrictive properties of BaTiO3 from first-principles. J. Appl. Phys. **108**, (2010) https://doi.org/10.1063/1.3462441
52. Koroglu, U., Cabuk, S., Deligoz, E.: Structural, electronic, elastic and vibrational properties of BiAlO3: a first principles study. J. Alloys Compd. **574**, 520–525 (2013)
53. Radjai, M., Guechi, N., Maouche, D.: An ab initio study of structural, elastic and electronic properties of hexagonal MAuGe (M = Lu, Sc) compounds, (2021). http://arxiv.org/abs/2103.15579. Accessed 29 Mar 2021
54. Ravindran, P., Fast, L., Korzhavyi, P.A., Johansson, B., Wills, J., Eriksson, O.: Density functional theory for calculation of elastic properties of orthorhombic crystals: application to TiSi2. J. Appl. Phys. **84**, 4891–4904 (1998). https://doi.org/10.1063/1.368733
55. Bao, L., Qu, D., Kong, Z., Duan, Y.: Anisotropies in elastic properties and thermal conductivities of trigonal TM2C (TM= V, Nb, Ta) carbides. Solid State Sci. **98**, 106027 (2019)
56. Voigt, W.: Lehrbuch der Kristallphysik, BB Teubner, Leipzig, 1928; b) A. Reuss. J. Appl. Math. Mech. **9**, 49–58 (1929)
57. Reuss, A.: Calculation of the flow limits of mixed crystals on the basis of the plasticity of monocrystals. Z Angew Math Mech. **9**, 49–58 (1929)
58. Hill, R.: The elastic behaviour of a crystalline aggregate. Proc. Phys. Soc. Sect. A. **65**, 349 (1952)
59. Radjai, M., Bouhemadou, A., Bitam, T.: First-principles investigation of the structural, elastic and thermodynamic properties of CaRu2X2 (X = P, As) under pressure. J. Supercond. Nov. Magn. **35**, 2531–2544 (2022). https://doi.org/10.1007/s10948-022-06304-7
60. Pugh, S.F.: XCII. Relations between the elastic moduli and the plastic properties of polycrystalline pure metals. Lond. Edinb. Dublin Philos. Mag. J. Sci. 45, 823–843 (1954). https://doi.org/10.1080/14786440808520496
61. Soh, J.W., Lee, H.M., Kwon, H.-S.: Relation between Poisson's ratio and ionicity in simple binary cubic compounds. J. Alloys Compd. **194**, 119–125 (1993)
62. Radjai, M., Essaoud, S.S., Bouhemadou, A., Allali, D., Bedjaoui, A., Bin-Omran, S., Khenata, R., Al-Douri, Y.: Computational investigation of the structural, elastic, electronic, and thermodynamic properties of chloroperovskites GaXCl3 (X= Be, Ca, or Sr) using DFT framework. Phys. Scr. **99**, 065917 (2024)